Edinburgh Research Explorer

Ciliary entry of the kinesin-2 motor KIF17 is regulated by importin-beta2 and RanGTP

Ciliary entry of the kinesin-2 motor KIF17 is regulated by importin-β2 and Ran-GTP

John F. Dishinger[1], **Hooi Lynn Kee**[1], **Paul M. Jenkins**[2], **Shuling Fan**[3], **Toby W. Hurd**[5], **Jennetta W. Hammond**[1], **Yen Nhu-Thi Truong**[2], **Ben Margolis**[3,4], **Jeffrey R. Martens**[2], and **Kristen J. Verhey**[1]

[1] Department of Cell and Developmental Biology, University of Michigan Medical School, Ann Arbor, Michigan 48109, USA

[2] Department of Pharmacology, University of Michigan Medical School, Ann Arbor, Michigan 48109, USA

[3] Department of Internal Medicine, University of Michigan Medical School, Ann Arbor, Michigan 48109, USA

[4] Department of Biological Chemistry, University of Michigan Medical School, Ann Arbor, Michigan 48109, USA

[5] Department of Pediatrics and Communicable Disease, Division of Pediatric Nephrology, University of Michigan Medical School, Ann Arbor, Michigan 48109, USA

Abstract

The biogenesis, maintenance, and function of primary cilia are controlled through intraflagellar transport (IFT) driven by two kinesin-2 family members, the heterotrimeric KIF3A/KIF3B/KAP complex and the homodimeric KIF17 motor[1,2]. How these motors and their cargoes gain access to the ciliary compartment is poorly understood. We identify a ciliary localization signal (CLS) in the KIF17 tail domain that is necessary and sufficient for ciliary targeting. Similarities between the CLS and classic nuclear localization signals (NLS) suggests that similar mechanisms regulate nuclear and ciliary import. We hypothesize that ciliary targeting of KIF17 is regulated by a Ran-GTP gradient across the ciliary base. Consistent with this, cytoplasmic expression of GTP-locked Ran(G19V) disrupts the gradient and abolishes ciliary entry of KIF17. Furthermore, KIF17 interacts with importin-β2 in a manner dependent on the CLS and inhibited by Ran-GTP. We propose that Ran plays a global role in regulating cellular compartmentalization by controlling the shuttling of cytoplasmic proteins into nuclear and ciliary compartments.

The development of the primary cilium, a microtubule-based organelle projecting from the surface of nearly all cells, has been proposed to be a consequence of evolved motor protein-based trafficking unique to eukaryotic cells[3]. Primary cilia play important roles in sensory functions such as photoreception, renal functioning, and odorant sensing at single- and

multicellular levels4⁻6. Defective biogenesis or functioning of cilia causes a variety of human diseases, collectively termed ciliopathies7,8, with pathological conditions including cystic kidney disease, brain malformations, and obesity.

Although able to respond to a variety of sensory stimulants, the basic structure of primary cilia is highly conserved. The core axoneme consists of a ring of nine doublet microtubules that extend from the mother centriole at the basal body1,9. Ciliary construction and maintenance proceeds through IFT of ciliary components along the axoneme by kinesin and dynein motors9. In *C. elegans*, IFT requires the coordinated efforts of heterotrimeric kinesin-2 (KIF3A/KIF3B/KAP complex) and homodimeric OSM-3 motors10,11. KIF17, the vertebrate homolog of OSM-3, has been shown to function as a ciliary motor in zebrafish photoreceptors and mammalian olfactory sensory neurons12⁻14.

How kinesin motors and their cargos gain entry to the cilium is unknown. Ciliary entry is a selective process as analysis across several species has identified a unique ciliary proteome15. Ciliary entry presumably requires the transport of proteins located near the basal body across the ciliary transition zone16 which may function as a diffusion barrier separating the cytoplasm from the intraciliary compartment. IFT cargo proteins have been observed around the basal body17 and transition fibers18 in the initial segment of cilia.

To study ciliary targeting of KIF17 in mammalian cells, we expressed mCitrine (mCit)-tagged KIF17 in cell lines that generate primary cilia. KIF17 accumulated at the distal tip of the primary cilium in all cell lines tested including neuronal (Odora rat olfactory sensory neurons19), epithelial (MDCKII canine kidney and hTERT-RPE human retinal pigment epithelia) and fibroblast (NIH3T3) cells (Fig. 1a). Localization to the distal cilium was confirmed by co-staining for acetylated and γ-tubulin to mark the cilium and basal body, respectively (Fig. 1b). Ciliary localization of tagged KIF17 was observed regardless of the epitope (mCit, FLAG, or myc) or its position (N- or C- terminal) (data not shown).

To identify sequences in KIF17 required for ciliary localization, we created truncated forms of the motor (Fig. 1c-e and Supplementary Fig. S1a). Deletion of the C-terminal tail domain abolished ciliary localization [KIF17(1-846), Fig. 1c], suggesting that the tail domain contains sequences required for ciliary targeting. Further C-terminal truncations also failed to localize to cilia (Supplementary Fig. S1). Surprisingly, constructs containing the KIF17 stalk and tail domains [mCherry-KIF17(490-1029), Fig. 1d] or the KIF17 tail domain alone [myc-KIF17(801-1028), Fig. 1e] localized predominantly to the nucleus (Fig. 1d,e). This suggests that similar mechanisms may control nuclear and ciliary targeting. Parallels between nuclear and ciliary import have been suggested in literature20⁻22, yet no direct evidence exists to date.

To explore the possibility that ciliary entry of KIF17 utilizes mechanisms similar to nuclear import, we searched KIF17 for sequences resembling an NLS23 and identified two potential sites: aa767-772 (KRRKR) and aa1016-1019 (KRKK). To test whether these sequences are necessary for KIF17 ciliary localization, we mutated the relevant residues to alanines in the full length motor (Fig. 1f,g). Mutation of residues 764-772 in the KIF17 stalk did not effect ciliary localization (Fig. 1f) whereas mutation of residues 1016-1019 in the KIF17 tail domain abolished ciliary localization (Fig. 1g). Identical results were obtained in other cell lines (Supplementary Fig. S2). These results indicate the KRKK sequence in the KIF17 tail domain acts as a CLS. The KIF17 CLS can also function as an NLS as mutation of residues 1016-1019 in the isolated KIF17 tail domain reduced the nuclear localization of this construct (Fig. 1e).

That the CLS is necessary for ciliary localization of KIF17 (Fig. 1g) but is not sufficient for ciliary targeting when present in the isolated tail domain (Fig. 1e) indicates that there are

likely to be several sequences in KIF17 that contribute to ciliary localization. To test whether the KIF17 CLS is sufficient for ciliary targeting of kinesin motors, we fused the tail domain (aa801-1028) onto the C-terminus of a non-ciliary kinesin, the Kinesin-1 subunit kinesin heavy chain (KHC) (Fig. 1h). Fusion of the wildtype KIF17 tail domain resulted in ciliary localization of KHC whereas fusion of the mutant KIF17 tail did not (Fig. 1h). This demonstrates that the KIF17 tail domain contains a CLS that is necessary and sufficient for ciliary targeting of kinesin motors.

Nuclear import involves recognition of NLSs by importin proteins, translocation through the nuclear pore complex (NPC), and dissociation of the NLS-importin complex in the nucleus by active GTP-bound forms of the small G-protein Ran[24]. To investigate whether similar mechanisms regulate ciliary import of CLS-containing KIF17, we tested whether Ran-GTP is present in primary cilia and regulates trafficking of KIF17. Ran and importin proteins are present in ciliary proteomes from several species[15,25]. We found that Ran is present in a ciliary fraction isolated from rat olfactory tissue (Fig. 2a). Isolation of a ciliary-enriched fraction was confirmed by the presence of the ciliary protein adenylyl cyclase III (Fig. 2a) and scanning electron microscopy (SEM) of olfactory tissue before and after cilia removal (Supplementary Fig. S3a). Immunohistochemistry of rat olfactory (Fig. 2b) and respiratory (Supplementary Fig. S3b) epithelia also demonstrates that Ran is present in the cilia layer at the apical surface. The ciliary-localized Ran represents the active GTP-bound state of the protein as both the cilium (Fig. 2c) and nucleus (Supplementary Fig. S4a) can be stained with an antibody that recognizes Ran-GTP but not Ran-GDP[26]. These results are consistent with our proposal that a RanGTP/GDP gradient across the ciliary/cytoplasmic barrier regulates ciliary import.

To test whether ciliary Ran-GTP regulates KIF17 import, we co-expressed KIF17-mCit with myc-tagged Ran proteins (WT, constitutively active GTP-bound G19V mutant, and T24N mutant that cannot bind nucleotide)[27]. We used serum-starved NIH3T3 cells in order to co-express the exogenous proteins after cilia formation and limit any effects of Ran overexpression on ciliogenesis. Cytoplasmic expression of WT or Ran(T24N) did not affect ciliary localization of KIF17 whereas expression of GTP-bound Ran(G19V) significantly reduced the number of cells with ciliary KIF17 without affecting cilia length (Supplementary Fig. S5).

To alleviate concerns that cytoplasmic expression of Ran proteins could indirectly affect ciliary targeting of KIF17, we developed a method for fast upregulation of Ran protein expression. The various Ran constructs were tagged with a destabilization-domain (DD) which targets expressed proteins for rapid degradation. Addition of the cell-permeable ligand Shield-1 prevents protein degradation and allows rapid and continuous upregulation of protein levels[28−30]. Our DD-Ran constructs were also tagged with the fluorescent protein Cerulean (Cer). To verify the rapid expression of Ran proteins, lysates of COS cells expressing the DD-Cer-Ran plasmids and exposed to Shield-1 for 0–8 h were analyzed by immunoblotting with a Ran antibody. Increasing exposure to Shield-1 resulted in increasing levels of DD-Cer-Ran with no change in endogenous Ran protein levels (Fig. 3a). In live cells, upregulation of DD-Cer-Ran protein expression can be observed after only 1 h of incubation with Shield-1 (Fig. 3b–d).

We then tested whether a rapid increase in cytoplasmic DD-Cer-Ran affected ciliary targeting of KIF17. NIH3T3 cells coexpressing KIF17-mCit and DD-Cer-Ran proteins were treated with Shield-1 for 0–4 h and then fixed and stained with antibodies to acetylated and γ-tubulins (Fig. 3e). After 4 h of Shield-1 treatment, increased expression of Ran(T24N) or WT Ran did not effect KIF17-mCit localization (Fig. 3e,f). However, increased expression of GTP-bound Ran(G19V) abolished ciliary localization of KIF17-mCit (Fig. 3e,f).

Interestingly, at shorter times of Shield-1 addition and DD-Cer-Ran(G19V) expression, KIF17-mCit localized to more proximal segments of the cilium and/or to the basal body (Figure 3e, bottom row). Similar results were obtained upon live imaging of cells expressing DD-Cer-Ran and monomeric red fluorescent protein (mRFP)-KIF17 constructs (Supplementary Fig. S6). Differences in DD-Cer-Ran(G19V) fluorescence intensity and nuclear localization between fixed (Fig. 3b) and live (Fig. 3e) cells are due to the methanol fixation/immunostaining procedure (Supplementary Fig. S4b). The loss of KIF17-mCit ciliary localization upon increased DD-Cer-Ran(G19V) expression is not due to Ran-GTP effects on cilia per se as no effect on the presence or length of cilia was observed (Fig. 3g,h). These results show that ciliary KIF17 is: 1) dynamic in its location and 2) mislocalized upon increased levels of cytoplasmic Ran-GTP. We suggest that cytoplasmic Ran-GTP abolishes ciliary entry of KIF17 while the dynamic process of IFT allows KIF17 already present in cilia to exit.

To directly test whether Ran controls ciliary entry of KIF17, we performed fluorescence recovery after photobleaching (FRAP) analysis of ciliary KIF17-mCit in the presence or absence of cytoplasmic DD-Cer-Ran(G19V). KIF17-mCit in the distal tips of Odora cilia was photobleached in a single confocal z-plane. In the absence of Shield-1, KIF17-mCit fluorescence in the distal tips of cilia recovered to pre-bleach levels within 20 min (Fig. 4a). After 1 h of Shield-1-induced upregulation of DD-Cer-Ran(G19V), little to no recovery of KIF17-mCit fluorescence in the cilium was observed (Fig. 4b). Comparison of fluorescence averages from multiple FRAP experiments revealed a drastic reduction in ciliary KIF17 recovery when Ran(G19V) levels were increased (Fig. 4c). We conclude that the presence of KIF17 in primary cilia is a steady-state process in which motor is entering and leaving the cilium with a constant accumulation at the distal tip, and that entry of KIF17 can be prevented by high levels of cytoplasmic Ran-GTP.

We next examined whether importin proteins play a role in ciliary entry of KIF17. In nuclear import, NLS-containing proteins form complexes with α- and/or β-importins and are shuttled into the nucleus through NPCs[24],[31]. We hypothesized that CLS-containing proteins complex with importins for transport across the ciliary transition zone. This possibility is supported by the presence of α/β-importins in ciliary proteomes from several species[15] and the interaction of the ciliary membrane protein Crumbs3 with importin-β1 during spindle assembly and ciliogenesis[32]. In Odora cells, importin-β2 localized near the nuclear envelope, as expected, as well as near the basal body and in the proximal region of the cilium, consistent with a role for importins in ciliary import (Fig. 5a). KIF17 interacts with importin-β2 as immunoprecipitation of Flag-KIF17 with anti-Flag antibodies resulted in coprecipitation of endogenous importin-β2 (Fig. 5b). The KIF17 CLS is critical for this interaction as importin-β2 was not coprecipitated with the 1016-1019ala mutant (Fig. 5b). That mutation of the KIF17 CLS (aa1016-1019) interfered with both ciliary entry (Fig. 1) and importin-β2 binding (Fig. 5b), indicates that interaction with importin-β2 is necessary for ciliary entry of KIF17. After crossing the ciliary transition zone, Ran-GTP in the cilium could dissociate KIF17 and importin-β2, freeing the motor for IFT. Indeed, addition of recombinant GST-Ran(G19V) to cell lysates prior to immunoprecipitation reduced the KIF17/importin-β2 interaction whereas addition of WT or Ran(T24N) had no effect (Fig. 5c).

As the primary sequence of the KIF17 CLS is similar to classical NLSs that interact with importin-β1, the interaction of KIF17 with importin-β2 was surprising. However, no interaction between KIF17 and importin-β1 was observed via immunoprecipitation (Fig. 5b). And similarities can be found between the KIF17 CLS and the basic-enriched/PY subclass of consensus sequences for importin-β2 binding[23]. To directly compare roles of importins β1 and β2 in ciliary entry of KIF17, we replaced the KIF17 CLS with NLSs

known to interact with either importin-β1 or importin-β2. KIF17-mCit still localized to primary cilia when its CLS was replaced with the M9 NLS from hnRNP A1, which interacts with importin-β2 (Fig. 5d). In contrast, KIF17-mCit was targeted to the nucleus when its CLS was replaced with the NLS from the SV-40 large T antigen, which interacts with importins α and β1 (Fig. 5d). These results suggest that importin-β2 alone is responsible for ciliary entry of KIF17.

In conclusion, we propose a model for ciliary import (Fig. 5e) in which cytoplasmic KIF17 interacts with importin-β2 (Fig. 5e′). This complex crosses the ciliary transition zone (Fig. 5e″) and is dissociated by Ran-GTP in the proximal cilium (Fig. 5e‴), allowing KIF17 to proceed with its role in IFT. Perturbation of the Ran-GTP/GDP gradient prevented ciliary entry of KIF17, presumably by inhibiting formation of KIF17/importin complexes before transport across the ciliary transition zone. These results provide the first direct evidence that ciliary and nuclear import pathways utilize similar mechanisms. In addition, Ran and importin proteins regulate the localization and activation of kinesin motors during spindle assembly in mitotic cells[33,34], and our work expands the role of Ran to include global regulation of kinesin compartmentalization in interphase cells.

How proteins gain access to the ciliary compartment has been unclear. Sequences critical for ciliary targeting of membrane proteins (e.g. VxPx, RVxP, Ax(S/A)xQ) are known[13,35,36] but it is unclear how these sequences function as several pathways have been described for trafficking of membrane proteins to the cilium[9, 37−39]. Here we describe a novel entry pathway for cytoplasmic kinesin motors analogous to nuclear entry of proteins. Whether importin- and Ran-regulated import pathways regulate entry of other motors and their cargoes at the ciliary transition zone requires further analysis.

It is interesting to note that the KIF17 CLS can function as a CLS or an NLS depending on protein context. Several NLS-like sequences have been found on the KIF3A/KIF3B/KAP complex, and the KAP subunit has been observed to redistribute from cilia nuclei during the mitotic cycle[40]. It is likely that additional signals in KIF17 are required to promote ciliary rather than nuclear import. One possiibility is that KIF17 motor activity along cytoplasmic and/or centriole microtubules is needed to position the CLS-containing protein at the ciliary base rather than the nuclear envelope. Alternatively, cargo and/or membrane binding may be required for ciliary entry. Further experiments are required to test these possibilities as well as the global role of importins and Ran in ciliary entry.

METHODS

Antibodies and plasmids

Commercial antibodies include: γ-tubulin (polyclonal and GTU-88 clone, Sigma), myc (9E10 clone, Sigma), importin-β2 (558660, BD Pharmingen), importin-β1 (610559, BD Transduction Laboratories), FLAG (F7425 or M2 clone, Sigma), Ran (610340, BD Transduction Laboratories), and adenylyl cyclase III (Santa Cruz Biotechnology). The rabbit polyclonal antibody to acetylated tubulin was raised against an acetylated α-tubulin peptide CGQMPSD(AcK)TIGGGDD. The rabbit anti-RanGTP antibody was a kind gift from Ian Macara (University of Virginia). Secondary antibodies for immunoblotting and immunofluorescence were from Jackson ImmunoResearch and Invitrogen.

Tagged versions of full length human KIF17 (NP_065867) were created in pmCit-N1 and pmCit-C11, pCDNA3-Flag, or pRK5-Myc using convenient restriction sites or PCR. Truncated versions were created by PCR using primers with appropriate restriction sites for subcloning back into the appropriate vector. All mutagenesis was performed using the Quickchange kit (Stratagene). Wildtype and mutant KIF17 tail domains were amplified by

PCR and inserted in frame between the KHC (rat KIF5C) and mCit coding sequences in the plasmid KHC-mCitN11. Plasmids for bacterial expression of wildtype and mutant Ran proteins were a gift from Brian Burke (University of Florida). The Ran coding sequences were subcloned into plasmids pCer-C1 and pRK5-Myc to create Cerulean and Myc-tagged versions, respectively, for expression in mammalian cells. The Destablization Domain (FKBP-L106P, Clontech Proteotuner System) was then inserted upstream of Cer to create the DD-Cer-Ran constructs.

Cell culture and transfection

MDCK II are dog kidney epithelial cells commonly utilized to study the formation and functioning of primary cilia. hTERT-RPE cells are from mouse retinal pigment epithelium immortalized with human telomerase. NIH3T3 are derived from NIH Swiss mouse embryo cultures. Odora cells are SV40-immortalized cells from rat olfactory epithelium.

Odora, NIH3T3, HEK293T, and COS cells were grown in DMEM (Gibco) supplemented with 10% fetal clone III (Hyclone) and 1% glutamax (Gibco). Cells were transfected using either Trans-IT (Mirus) or ExpressFect (Denville) transfection reagents and typically used for experiments 24 h after transfection. NIH3T3 cells were serum starved for 24 – 48 h to induce ciliogenesis prior to transfection. MDCK II cells were grown in DMEM supplemented with 10% FBS and 1% Glutamax, and transfected using Lipofectamine (Invitrogen) in Opti-MEM (Gibco). hTERT-RPE cells were grown in DMEM/F12 media (Gibco) supplemented with 10% FBS and 0.01 mg/mL hygromycin B, transfected with Trans-IT transfection reagent, and serum starved for 24 – 48 h to induce ciliogenesis.

Isolation of cilia from rat olfactory epithelium

Female Sprague-Dawley rats were obtained from Harlan (Indianapolis, IN) and were used in the pisolation of primary cilia from the rat olfactory epithelium. All experimental procedures were approved by the University of Michigan Committee on the Use and Care of Animals and performed in accordance with the Guide for the Care and Use of Laboratory Animals, as adopted and promulgated by the National Institutes of Health.

Olfactory cilia were isolated using a combination of the "calcium-shock" method[2] followed by NaBr treatment[3] with minor modifications. The olfactory epithelia from seven rats were surgically removed, washed in ice-cold Ringer's Solution [120mM NaCl, 5mM KCl, 1.6mM K_2HPO_4, 25mM $NaHCO_3$, 7.5mM D-glucose, 5mM EGTA], and then placed in deciliation solution [Ringer's Solution containing complete protease inhibitor cocktail (Roche Applied Science, Indianapolis, IN), 20mM $CaCl_2$ and 30mM KCl]. Cilia were detached by gentle agitation for 20 min at 4°C and isolated by multiple centrifugation steps in a 45% w/v sucrose solution. Cilia visible as a white layer at the sucrose-supernatant interface were extracted and diluted in ten-fold volume of deciliation solution and then pelleted. The cilia pellet was resuspended in a NaBr solution then centrifuged again. This was repeated once more before the final cilia pellet was resuspended in washing solution (10mM Tris, 3mM $MgCl_2$, 2mM EGTA), centrifuged a final time, and then analyzed by SDS-PAGE and Western blot.

Deciliated lysates were prepared from tissue remaining after deciliation. The tissue was homogenized using a dounce homogenizer in deciliation solution. Insoluble material was removed by centrifugation and supernatant portions were analyzed by SDS-PAGE and Western blot.

Deciliation was verified by SEM. Olfactory epithelia were removed from euthanized animals, washed in ice-cold Ringer's Solution, and either immediately placed in fixative solution (8% glutaraldeheyde, 0.6M cacoydylate, H_2O) for 24 h at 4°C or deciliated by

gentle agitation in deciliation solution and then subsequently placed in fixative solution for 24 h at 4°C. Epithelia were then processed using the OTOTO method4. Samples were dehydrated in a graded series of increasing ethanol concentrations, critical point dried, and mounted on stubs using silver paste. Samples were analyzed using an AMRAY 1910 Field Emission Scanning Electron Microscope (FEG-SEM).

Immunofluorescence and immunohistochemistry

For immunofluorescence, cells were fixed in either methanol at −20°C or 3.7% PFA followed by 50 mM NH_4Cl at room temperature. Samples were permeabilized with 0.2% TX-100 for 5 min and then briefly blocked with 0.2% fish skin gelatin (Sigma) in PBS before addition of primary and secondary antibodies. For immunostaining with the anti-Ran-GTP antibody, cells were permeabilized with 0.05% TX-100 to allow for good visualization of ciliary-localized proteins. Permeabilization with higher levels of TX-100 (0.1 or 0.25%) allowed for nuclear staining (Supplementary Fig. S5b), but somewhat inhibited visualization of RanGTP in the ciliary compartment.

For immunohistochemistry, olfactory epithelia were removed from animals euthanized by cardiac perfusion with PBS followed by 4% paraformaldehyde, post-fixed in 4% paraformaldeheyde for 4 h, and then incubated in 30% sucrose solution for 24 h at 4°C. After incubation, samples were frozen in OCT compound (Sakura Finetek, Torance, CA) and cut into sections (20 micron) on a cryostat. Epithelium tissue was incubated with 1% SDS for 10 min and washed with PBS before incubation with primary and secondary antibodies.

All samples were mounted with ProLong Gold (Invitrogen). Images were obtained on an inverted epi-fluoresence microscope (TE2000-E, Nikon) or a confocal imaging system (FluoView 500, Olympus) and analyzed with ImageJ (NIH) or MetaMorph software (Molecular Devices). Tissue images were obtained by taking a series of z-series every 0.5 μm through the epithelium and combining the images into a composite stack.

Immunoprecipitation

HEK293T cell lysate was prepared in lysis buffer (25 mM HEPES, 115 mM KOAc, 5 mM NaOAc, 5 mM Mgcl2, 0.5 mM EGTA, 1% TX-100) and protease inhibitors (1mM). Lysates were cleared twice before addition of antibody alone or 5 μg recombinant Ran proteins at 4°C. Immunoprecipitates were recovered with protein A agarose beads (Invitrogen), washed at least twice in lysis buffer, and analyzed by SDS-PAGE and western blotting.

Purification of bacterially expressed proteins

Expression of GST-tagged Ran-WT, G19V, and T24N proteins in BL21 (DE3) cells was induced with 100 μM IPTG for 2 h at 37°C. After lysis, the GST-tagged proteins were purified using Glutathione Sepharose beads (GE Healthcare). Purified proteins were dialyzed overnight in 10 mM Tris pH 7.4, 150 mM NaCl, 1 mM EDTA, 1 mM DDT, and 5% glycerol. Protein concentration was determined by Bradford assay.

DD-Ran experiments

For fixed cell experiments, serum starved NIH3T3 cells were transfected with DD-Cer-Ran and KIF17 constructs for 24 h before addition of Shield-1 for 0 – 4 h, then fixed, permeabilized, and immunostained. Cilium lengths were determined with MetaMorph software by tracing the midline of primary cilia visualized with acetylated tubulin antibody.

For live cell DD-Ran experiments, cells were plated in glass bottom dishes (MatTek), serum starved for 24 – 48 h, and then transfected. Immediately before imaging, cells were put into

a pre-warmed HEPES buffer (25 mM HEPES, 115 mM KOAc, 5 mM NaOAc, 5 mM MgCl$_2$, 2 mM EGTA) supplemented with Shield-1. Cells chosen for experiments were morphologically normal and presented good expression of KIF17 along the length of primary cilia. An objective heater (Bioptechs) was used to warm cells. Images were taken every 10 min for up to 4 h and analyzed with ImageJ.

For FRAP experiments, Odora cells in glass-bottomed dishes expressing KIF17-mCit and DD-Cer-Ran(G19V) were imaged on an Olympus FluoView confocal system using a live cell imaging chamber to maintain appropriate temperature and atmosphere. Cells were imaged either before or 1 h after the addition of Shield-1 directly to cell media. Distal tips of cilia were photobleached using 100% laser power for 90s, and recovery images were taken at 1 min intervals for 20 min at 10% laser power. Fluorescence data was subjected to background subtraction and normalized for additional photobleaching during recovery. Averaged data was plotted and fitted to single exponential functions in Prism software (Graphpad Software).

Statistical analysis

All statistical analysis was performed using Prism software and specific tests are noted in the text. Unless otherwise noted, all error bars represent ± SEM and significance was assessed as $p < 0.05$.

Supplementary Material

Refer to Web version on PubMed Central for supplementary material.

Acknowledgments

REFERENCES (MAIN TEXT)

1. Silverman MA, Leroux MR. Intraflagellar transport and the generation of dynamic, structurally and functionally diverse cilia. Trends Cell Biol. 2009; 19:306–316. [PubMed: 19560357]

2. Scholey JM. Intraflagellar transport motors in cilia: moving along the cell's antenna. J Cell Biol. 2008; 180:23–29. [PubMed: 18180368]

3. Satir P, Mitchell DR, Jekely G. How Did the Cilium Evolve? Ciliary Function in Mammalian Development. 2008; 85:63–82.

4. Gerdes JM, Davis EE, Katsanis N. The Vertebrate Primary Cilium in Development, Homeostasis, and Disease. Cell. 2009; 137:32–45. [PubMed: 19345185]

5. Satir P, Christensen ST. Overview of structure and function of mammalian cilia. Annu Rev Physiol. 2007; 69:377–400. [PubMed: 17009929]

6. Scholey JM, Anderson KV. Intraflagellar transport and cilium-based signaling. Cell. 2006; 125:439–442. [PubMed: 16678091]

7. Tobin JL, Beales PL. The nonmotile ciliopathies. Genet Med. 2009; 11:386–402. [PubMed: 19421068]

8. Fliegauf M, Benzing T, Omran H. Mechanisms of disease - When cilia go bad: cilia defects and ciliopathies. Nat Rev Mol Cell Bio. 2007; 8:880–893. [PubMed: 17955020]

9. Rosenbaum JL, Witman GB. Intraflagellar transport. Nat Rev Mol Cell Bio. 2002; 3:813–825. [PubMed: 12415299]

10. Ou GS, Blacque OE, Snow JJ, Leroux MR, Scholey JM. Functional coordination of intraflagellar transport motors. Nature. 2005; 436:583–587. [PubMed: 16049494]

11. Snow JJ, et al. Two anterograde intraflagellar transport motors cooperate to build sensory cilia on C-elegans neurons. Nat Cell Biol. 2004; 6:1109–U1123. [PubMed: 15489852]

12. Insinna C, Pathak N, Perkins B, Drummond I, Besharse JC. The homodimeric kinesin, Kif17, is essential for vertebrate photoreceptor sensory outer segment development. Dev Biol. 2008; 316:160–170. [PubMed: 18304522]

13. Jenkins PM, et al. Ciliary targeting of olfactory CNG channels requires the CNGB1b subunit and the kinesin-2 motor protein, KIF17. Curr Biol. 2006; 16:1211–1216. [PubMed: 16782012]

14. Insinna C, Humby M, Sedmak T, Wolfrum U, Besharse JC. Different Roles for KIF17 and Kinesin II in Photoreceptor Development and Maintenance. Dev Dynam. 2009; 238:2211–2222.

15. Gherman A, Davis EE, Katsanis N. The ciliary proteome database: an integrated community resource for the genetic and functional dissection of cilia. Nat Genet. 2006; 38:961–962. [PubMed: 16940995]

16. Gilula NB, Satir P. Ciliary Necklace - Ciliary Membrane Specialization. J Cell Biol. 1972; 53:494. [PubMed: 4554367]

17. Luby-Phelps K, Fogerty J, Baker SA, Pazour GJ, Besharse JC. Spatial distribution of intraflagellar transport proteins in vertebrate photoreceptors. Vision Res. 2008; 48:413–423. [PubMed: 17931679]

18. Deane JA, Cole DG, Seeley ES, Diener DR, Rosenbaum JL. Localization of intraflagellar transport protein IFT52 identifies basal body transitional fibers as the docking site for IFT particles. Curr Biol. 2001; 11:1586–1590. [PubMed: 11676918]

19. Murrell JR, Hunter DD. An olfactory sensory neuron line, Odora, properly targets olfactory proteins and responds to odorants. J Neurosci. 1999; 19:8260–8270. [PubMed: 10493727]

20. Jekely G, Arendt D. Evolution of intraflagellar transport from coated vesicles and autogenous origin of the eukaryotic cilium. Bioessays. 2006; 28:191–198. [PubMed: 16435301]

21. Devos D, et al. Components of coated vesicles and nuclear pore complexes share a common molecular architecture. PLOS biol. 2004; 2:2085–2093.

22. Christensen ST, Pedersen LB, Schneider L, Satir P. Sensory cilia and integration of signal transduction in human health and disease. Traffic. 2007; 8:97–109. [PubMed: 17241444]

23. Lee BJ, et al. Rules for nuclear localization sequence recognition by karyopherin beta 2. Cell. 2006; 126:543–558. [PubMed: 16901787]

24. Stewart M. Molecular mechanism of the nuclear protein import cycle. Nat Rev Mol Cell Bio. 2007; 8:195–208. [PubMed: 17287812]

25. Liu Q, et al. The proteome of the mouse photoreceptor sensory cilium complex. Mol Cell Proteomics. 2007; 6:1299–1317. [PubMed: 17494944]

26. Richards SA, Lounsbury KM, Macara IG. The C Terminus of the Nuclear RAN/TC4 GTPase Stabilizes the GDP-bound State and Mediates Interactions with RCC1, Ran-GAP, and HTF9A/RanBP1. J Biol Chem. 1995; 270:14405–14411. [PubMed: 7782302]

27. Lounsbury KM, Richards SA, Carey KL, Macara IG. Mutations within the Ran/TC4 GTPase - Effects on regulatory factor interactions and subcellular localization. J Biol Chem. 1996; 271:32834–32841. [PubMed: 8955121]

28. Banaszynski LA, Chen LC, Maynard-Smith LA, Ooi AGL, Wandless TJ. A rapid, reversible, and tunable method to regulate protein function in living cells using synthetic small molecules. Cell. 2006; 126:995–1004. [PubMed: 16959577]

29. Maynard-Smith LA, Chen LC, Banaszynski LA, Ooi AGL, Wandless TJ. A directed approach for engineering conditional protein stability using biologically silent small molecules. J Biol Chem. 2007; 282:24866–24872. [PubMed: 17603093]

30. Schoeber JPH, et al. Conditional fast expression and function of multimeric TRPV5 channels using Shield-1. Am J Physiol Renal Physiol. 2009; 296:F204–F211. [PubMed: 18842822]

31. Weis K. Regulating access to the genome: Nucleocytoplasmic transport throughout the cell cycle. Cell. 2003; 112:441–451. [PubMed: 12600309]

32. Fan SL, et al. A novel Crumbs3 isoform regulates cell division and ciliogenesis via importin beta interactions. J Cell Biol. 2007; 178:387–398. [PubMed: 17646395]

33. Ems-McClung SC, Zheng YX, Walczak CE. Importin alpha/beta and Ran-GTP regulate XCTK2 microtubule binding through a bipartite nuclear localization signal. Mol Biol Cell. 2004; 15:46–57. [PubMed: 13679510]

34. Tahara K, et al. Importin-beta and the small guanosine triphosphatase Ran mediate chromosome loading of the human chromokinesin Kid. J Cell Biol. 2008; 180:493–506. [PubMed: 18268099]

35. Mazelova J, et al. Ciliary targeting motif VxPx directs assembly of a trafficking module through Arf4. EMBO J. 2009; 28:183–192. [PubMed: 19153612]

36. Geng L, et al. Polycystin-2 traffics to cilia independently of polycystin-1 by using an N-terminal RVxP motif. J Cell Sci. 2006; 119:1383–1395. [PubMed: 16537653]

37. Pazour GJ, Bloodgood RA. Targeting Proteins to the Ciliary Membrane. Curr Top Dev Biol. 2008; 85:115–149. [PubMed: 19147004]

38. Hunnicutt GR, Kosfiszer MG, Snell WJ. Cell Body and Flagellar Agglutinins in Chlamydomonas-Reinhardtii - the Cell Body Plasma-Membrane Is a Reservoir for Agglutinins Whose Migration to the Flagella Is Regulated by a Functional Barrier. J Cell Biol. 1990; 111:1605–1616. [PubMed: 2170424]

39. Casanova JE, et al. Association of Rab25 and Rab11a with the apical recycling system of polarized Madin-Darby canine kidney cells. Mol Biol Cell. 1999; 10:47–61. [PubMed: 9880326]

40. Morris RL, et al. Redistribution of the kinesin-II subunit KAP from cilia to nuclei during the mitotic and ciliogenic cycles in sea urchin embryos. Dev Biol. 2004; 274:56–69. [PubMed: 15355788]

REFERENCES (METHODS SECTION)

1. Cai DW, Hoppe AD, Swanson JA, Verhey KJ. Kinesin-1 structural organization and conformational changes revealed by FRET stoichiometry in live cells. J Cell Biol. 2007; 176:51–63. [PubMed: 17200416]

2. Mayer U, et al. Proteomic analysis of a membrane preparation from rat olfactory sensory cilia. Chem Senses. 2008; 33:145–162. [PubMed: 18032372]

3. Mayer U, et al. The proteome of rat olfactory sensory cilia. Proteomics. 2009; 9:322–334. [PubMed: 19086097]

4. Davies S, Forge A. Preparation of the Mammalian Organ of Corti for Scanning Electron-Microscopy. J Microsc-Oxford. 1987; 147:89–101.
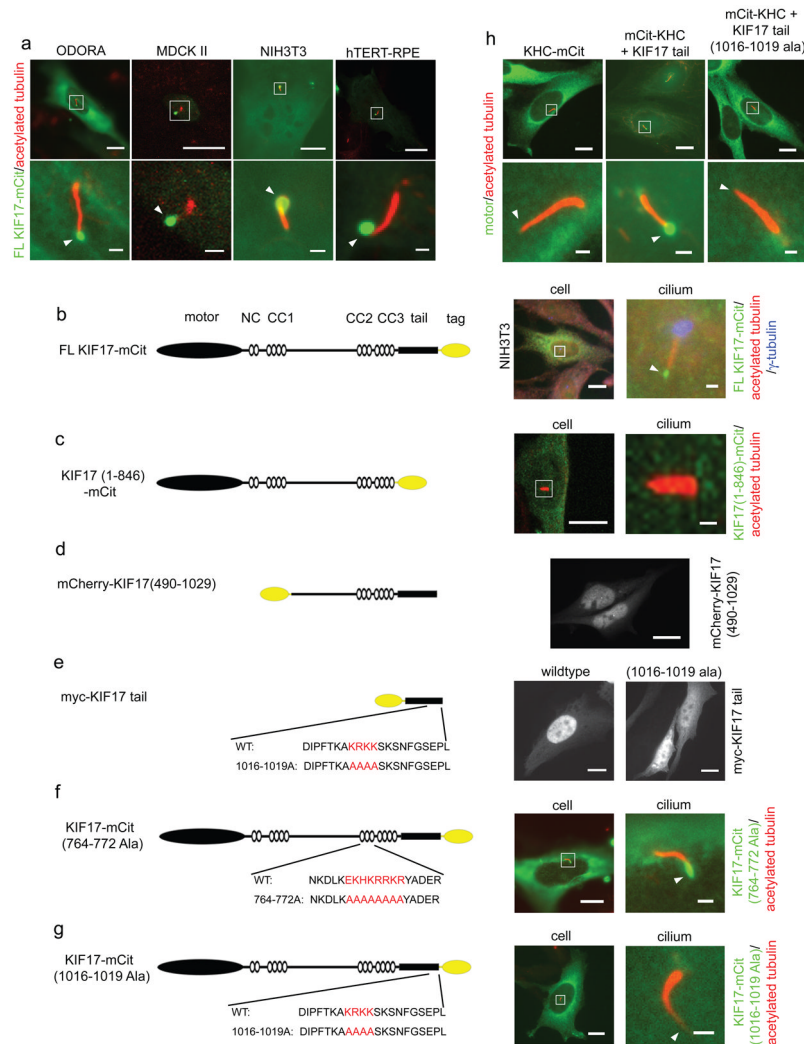
Figure 1.
The KIF17 CLS is necessary and sufficient for ciliary localization. (**a**) Odora, MDCK II, NIH3T3, and hTERT-RPE cells expressing full length KIF17-mCit (green) were fixed and stained for acetylated tubulin to mark cilia (red). Top row, images of entire cells; bottom row, higher magnification of cilia in boxed areas. White arrowheads indicate distal tips of cilia. (**b**) Left, schematic of full length human KIF17. NC, neck coil; CC, coiled-coil. Right, NIH3T3 cells expressing KIF17-mCit (green) were fixed and stained for acetylated tubulin (red) to mark cilia and γ-tubulin (blue) to mark the basal body. (**c-g**) Schematics of truncated and mutant KIF17 constructs (left) and their localization in Odora cells (right). Cells expressing the indicated truncated or mutant KIF17 motors (green) were fixed and stained for acetylated tubulin (red in c,f,g) or the myc tag (white in d). (**h**) Odora cells expressing full length KHC-mCit or KHC fused with the wildtype or mutant versions of the KIF17 tail were fixed and stained with antibodies to acetylated tubulin (red). Scale bars throughout figure are either 10 μm for images of entire cell or 1 μm for cilia.
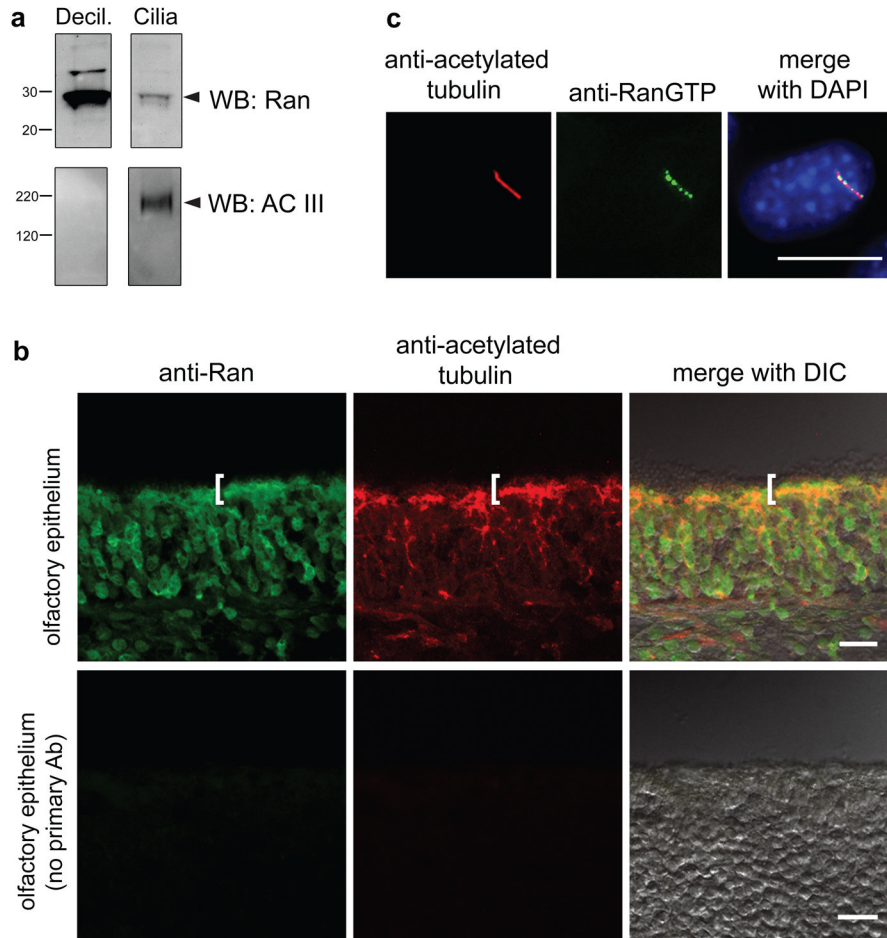
Figure 2.
Ran is present in the ciliary compartment. (**a**) Primary cilia were isolated from rat olfactory epithelium and the presence of Ran and adenylyl cyclase III (ACIII) in the ciliary (Cilia) and remaining deciliated (Decil.) fractions were determined by western blotting. Approximate molecular weights shown on left (kDa). Arrowheads designate protein of interest. Uncropped images of western blots are shown in Supplementary Fig. S7. (**b**) Representative compressed confocal stacks of coronal sections of rat nasal epithelia. Olfactory epithelia were immunostained with antibodies directed against Ran (left, green) and acetylated tubulin (middle, red). Merged imaged with Differential Interference Contrast (DIC) image is shown on right. Scale bar, 20 μm. Brackets denote cilia layer. Control images without primary antibody are shown in second row. (**c**) Immunofluorescence image of an NIH3T3 cell stained with anti-acetylated tubulin antibody (red), anti-RanGTP antibody (green), and DAPI (blue). Scale bar, 10 μm.
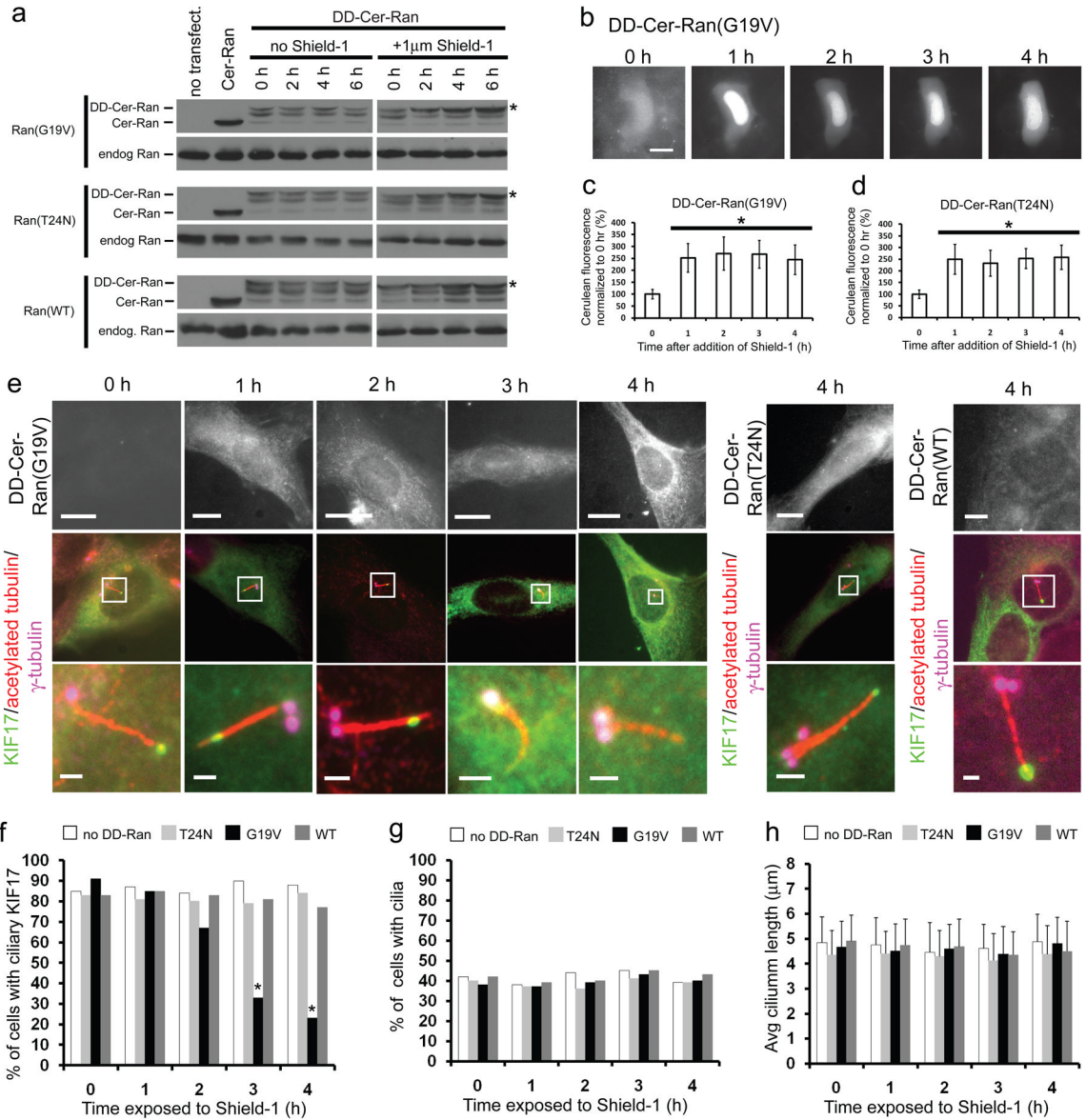
Figure 3.
Fast upregulation of cytosolic Ran-GTP levels abolishes ciliary localization of KIF17. (**a**) COS cells expressing Cer-Ran (G19V, T24N, and WT), DD-Cer-Ran(G19V, T24N, or WT) or untransfected control cells were exposed to Shield-1 for 0 – 8 h (right panels) or untreated (left panels). The expression of endogenous and expressed Ran was determined by immunoblotting with an anti-Ran antibody. Uncropped images of western blots are shown in Supplementary Fig. S7. (**b-d**) Single cell analysis of live NIH3T3 cells expressing DD-Cer-Ran constructs upon exposure to Shield-1. (**b**) Representative images of a single cell expressing DD-Cer-Ran(G19V) at 0–4 h of Shield-1 exposure. Scale bar, 10 μm. The fluorescence increase in multiple cells was quantified for (**c**) DD-Cer-Ran(G19V) expressing cells (*n*=8) and (**d**) DD-Cer-Ran(T24N) expressing cells (*n*=10). Quantification includes both nuclear and cytoplasmic fluorescence. *, p<0.05 as compared to 0 h time point (two-tailed Student's t-test). Data are presented as mean ± SEM. (**e**) NIH3T3 cells coexpressing KIF17-mCit and DD-Cer-Ran(WT) (right), DD-Cer-Ran(G19V) (left), or DD-Cer-Ran(T24N) (middle) were exposed to Shield-1 for 0–4 h and then fixed and stained for

acetylated tubulin and γ-tubulin. (**f-h**) Quantification of the results in (e) to determine (**f**) the percentage of transfected cells with ciliary localization of KIF17-mCit (n=30 for each time point, collected over 3 experiments), (**g**) the percentage of transfected cells with cilia (n=50 for each), and (**h**) the cilium length in transfected cells (n=30 for each). *, p<0.05 as compared to 0 h of Shield-1 (Fisher's Exact test). Data are presented as mean ± SD.
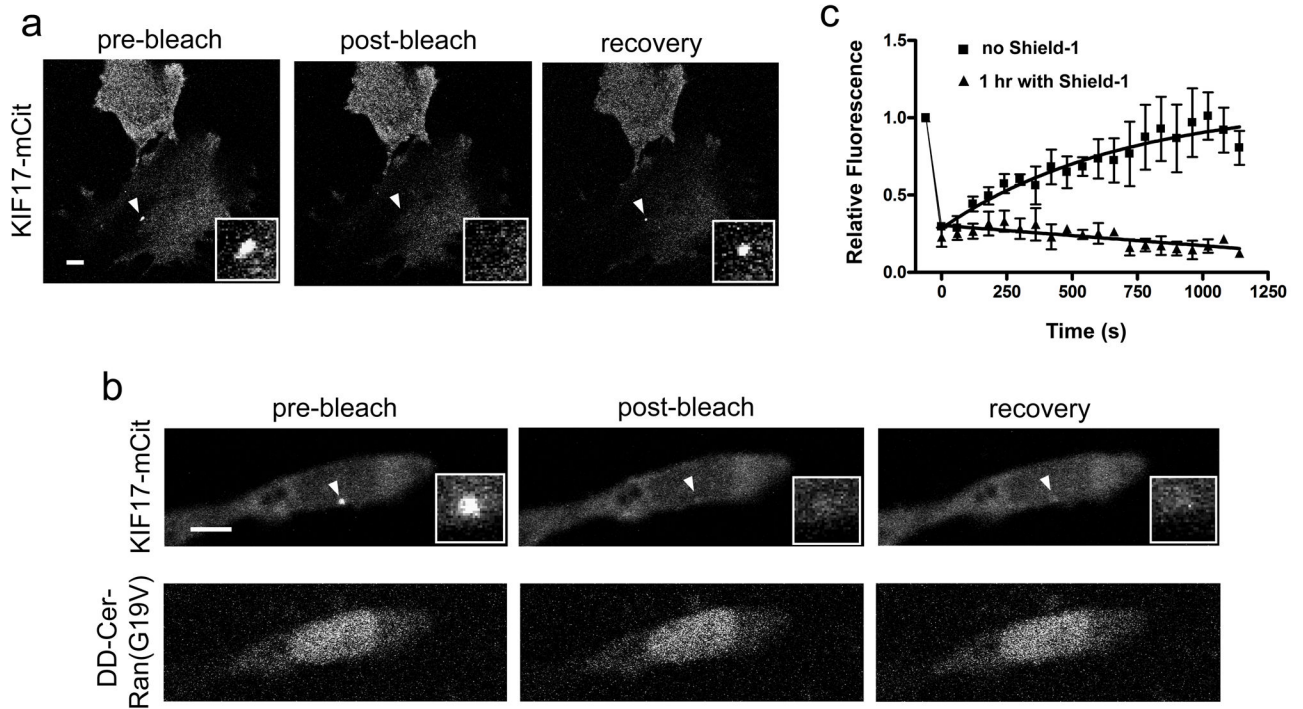
Figure 4.
Upregulation of cytosolic Ran-GTP levels prevents ciliary entry of KIF17. FRAP analysis of Odora cells coexpressing KIF17-mCit and DD-Cer-Ran(G19V) in the (**a**) absence or (**b**) presence of Shield-1. The cells were imaged (pre-bleach) and then the fluorescence in the distal tip of the cilium was bleached at high laser power. The cells were again imaged (post-bleach) and the fluorescence recovery of KIF17-mCit in the cilium was monitored over time. White arrowheads, distal tips of cilia. Inset of each image is a close up of the cilium tip. Scale bars are 10 μm. (**c**) The fluorescence recovery of KIF17-mCit in the distal tips of cilia in the absence and presence of Shield-1 was quantified. Data are presented as mean $\pm$ SEM. n=5 for both traces. Data were subjected to single exponential curve fits.
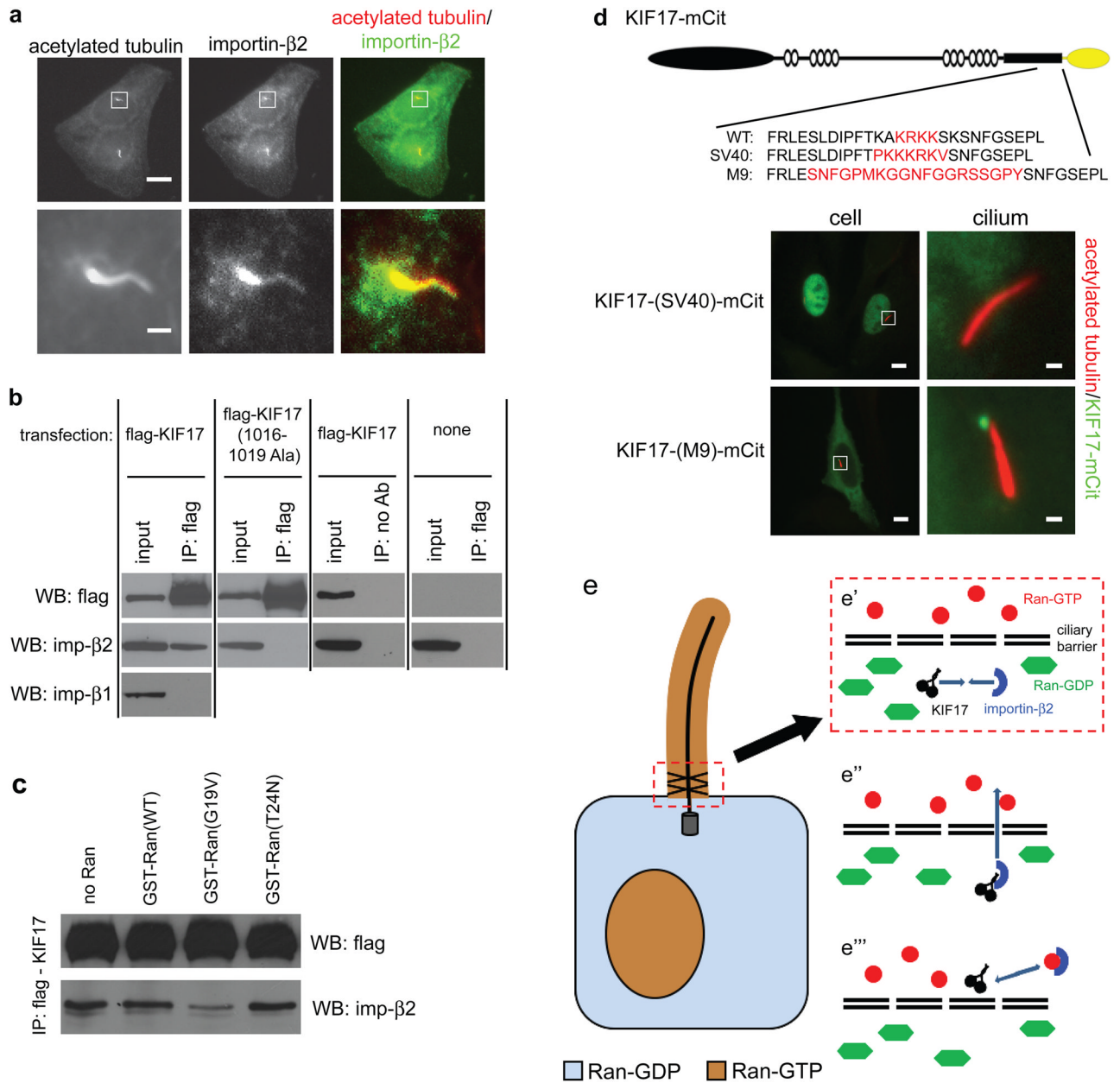
Figure 5.
KIF17 forms a complex with importin-β2 that is CLS- and Ran-GTP-dependent. (**a**) Odora cells were fixed and stained with antibodies to importin-β2 and acetelyated tubulin. Top row, images of entire cells; scale bar, 10 μm. Bottom row, magnification of boxed region containing cilia; scale bar, 1 μm. (**b**) Lysates of HEK293T cells expressing Flag-KIF17 or Flag-KIF17(1016-1019ala) or untransfected cells were immunoprecipitated with an anti-Flag antibody. The presence of expressed Flag-KIF17 and endogenous importin-β1 and -β2 proteins in the precipitates was probed by immunoblotting. (**c**) Lysates of HEK293T cells expressing Flag-KIF17 were immunoprecipitated with an anti-FLAG antibody in the absence (no Ran) or presence of the indicated purified GST-Ran proteins. The presence of expressed Flag-KIF17 and endogenous importin-β2 proteins in the precipitates was detected by immunoblotting. Uncropped images of western blots are shown in Supplementary Fig.

S7. (**d**) (Left) Schematic of KIF17-mCit constructs in which the CLS is replaced with the NLS from SV40 T-antigen or the M9 NLS from hnRNP A1. (Right) Images of Odora cells expressing KIF17-mCit SV40 or M9 constructs and stained with anti-acetylated tubulin antibody. Scale bar, 1 or 10 μm. (**e**) Model for ciliary import of KIF17. In the cytoplasm (**e**′), KIF17 interacts with importin-β2 in a manner dependent on the KIF17 CLS. The importin/KIF17 complex is able to shuttle across the ciliary transition zone (**e**″) and into the cilium. Once across the barrier (**e**‴), the high levels of Ran-GTP in the cilium cause a dissociation of the KIF17-importin-β2 complex, allowing KIF17 to proceed with its role in IFT. Brown shading, subcellular areas of high RanGTP. Blue shading, subcellular areas of high Ran-GDP.